Differential Flatness-Based, Full-Order Nonlinear Control of a Modular Multilevel Converter (MMC)

Pierre-Baptiste Steckler, Jean-Yves Gauthier, Xuefang Lin-Shi, Francois Wallart

Differential flatness based, full-order nonlinear control of a Modular Multilevel Converter (MMC)

Pierre-Baptiste Steckler, Jean-Yves Gauthier, Xuefang Lin-Shi, and François Wallart

***Abstract*—Modular Multilevel Converter (MMC) is an attractive topology in industrial applications such as high voltage direct current (HVDC) transmission system where a fast power control is required. The most conventional control method for MMC uses cascaded structures, where the power transmission and internal energy dynamic (outer loops) is limited by the "frequency separation" constraints, since the dynamic choice of the currents (inner loops) must take into account the tradeoff between rapidity and robustness. In this paper, we present a new control method based on differential flatness theory. The main interest of the proposed control is the possibility to obtain very high dynamic performance of the MMC power flow, even under noisy measurements and parametric disturbances. Using the well-known average model of the MMC, a flat output is proposed, proving the differential flatness property of the MMC. Trajectory tracking controllers of AC grid active and reactive power are proposed using input-state full-order linearization. Simulation results including losses corresponding to a realistic case of on-shore, point-to-point HVDC interconnection are presented to show the performance of the proposed control scheme even with strong measurement noise.**

***Index Terms*—Flatness, non-linear control, state-input linearization, trajectory planning, MMC, HVDC, multi-level inverter, power converter**

I. Introduction

As the share of renewable energy and the need for flexibility are constantly growing, transporting large amounts of energy at low cost and with low losses becomes mandatory. To achieve this goal, the High Voltage Direct Current (HVDC) technology, especially through its Voltage Source Converter (VSC) branch, appears today as a reference. However, despite their multiple advantages, DC grids have a major drawback: their inertia is extremely low compared to AC transmission systems [1]. From the need of stabilization of these high-level systems comes a need for fast and accurate converter-side control strategies.

This work was supported by a grant overseen by the French National Research Agency (ANR) as part of the "Investissements d'Avenir" Program (ANE-ITE-002-01).

P.-B. Steckler is with SuperGrid Institute SAS, Villeurbanne, 69628 France and Université de Lyon, INSA Lyon, Ampère, Villeurbanne, 69621, France. e-mail: pierre-baptiste.steckler@supergrid-institute.com

J.-Y. Gauthier is with SuperGrid Institute SAS, Villeurbanne, 69628 France and Université de Lyon, INSA Lyon, Ampère, Villeurbanne, 69621, France. e-mail: jean-yves.gauthier@insa-lyon.fr

X. Lin-Shi is with SuperGrid Institute SAS, Villeurbanne, 69628 France and Université de Lyon, INSA Lyon, Ampère, Villeurbanne, 69621, France. e-mail: xuefang.shi@insa-lyon.fr

F. Wallart is with SuperGrid Institute SAS, Villeurbanne, 69628 France e-mail: francois.wallart@supergrid-institute.com

Compared to the traditional High Voltage Alternating Current (HVAC) solution, a converter is needed at each end of the transmission line, but the kilometric cost is much lower. Other HVDC technologies are available, like the former Line-Commutated Converter (LCC). Whereas the LCC has a lower cost, higher efficiency and higher reliability, it has several drawbacks compared to the VSC. The latter offers a better controllability (separated active/reactive power control), a better energy quality (low harmonics generation without filtering) and can be extended to multi-terminal (meshed) grids easily. Many VSC structures were proposed, but the most used is certainly the Modular Multilevel Converter (MMC) [2], which has been invented in 2001. In Fig. 1, a three-phase MMC is presented in its half-bridge version. It consists of three parallel-connected phase legs each contains an upper arm and a lower arm. Each arm is constituted by a few hundreds of sub-modules (SMs), series-connected with an air-core reactor.

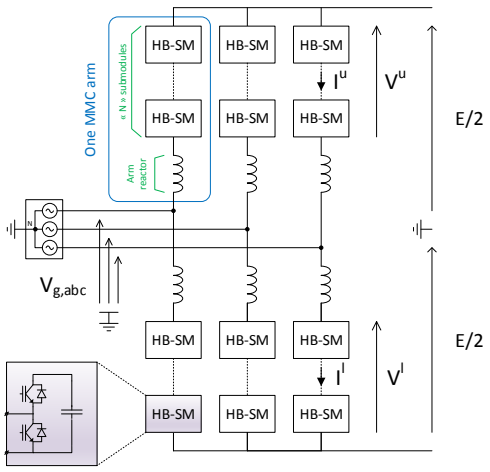

Fig. 1. MMC schematic including half-bridge submodules (HB-SM)

One drawback of the MMC compared to the former technologies, including previous VSC generations, lies in its modeling and control complexity. The most conventional control design of MMC can be separated in two main parts: a high level control which controls power exchanges inside the MMC depending on the mode operation and the control goal, and a low level control called capacitor voltage "Balancing Control Algorithm" [3] [4], whose goal is to generate the switch control signals to select the appropriate SMs to be inserted in order to balance their voltages. This paper focuses only on the high level control. Even if the so-called "average model" is used [5], greatly reducing the state variables count from a few hundreds to 12 (6 arm inductor currents and 6

equivalent capacitor voltages), it is still a high-order, Multi-Input Multi-Output (MIMO) non-linear system. This often leads to complex control schemes including a large number of tuning parameters with non-straightforward impact on the system behavior. The use of cascaded control [6] [7], which constitutes the most common solution, includes the outer loops (AC power, DC power and SM energy loops) and the inner loops (AC and DC current loops). It is convenient from several point of views, but comes with an inherent slowness, as it forces the use of very fast inner loops to obtain a decent rapidity on the outer ones. This need of fastness exposes the control scheme to noise sensitivity and decreases its overall robustness. As introduced before, the control of high-power, grid-connected converters is challenging, because the overall grid stability relies on fast and robust local controllers. Consequently, a non-linear control system is presented here, which allows a better tradeoff between tracking performance and noise robustness.

Different class of control laws can be used to ensure stability of non-linear systems, as the Lyapunov-based methods like Backstepping [8], but the fulfillment of a given performance indicator, based on response time or overshoot for instance, is more difficult. A convenient way to satisfy this constraint is the use of linearizing control. Feedback linearization is certainly an option, but in the case of MMC, it leads to the apparition of a so-called zero dynamics [9]. This has several drawbacks: not the whole state vector is linearized, a parasitic non-linear dynamics appears, and cascade control is still needed to satisfy all the control objectives, with the consequences given previously.

An interesting candidate to solve this control problem is based on Differential Flatness Theory (DFT). This principle has been applied to many complex nonlinear systems, such as fluid-powered actuators [10], power electronics [11] [24] or electro-mechanical systems [12] [13]. An overview of its application to the field of power electronics can be found in [14]. It comes with the following strengths:

1) Naturally adapted to trajectory tracking
2) Fast response possible with low overall loop gain
3) Low tuning parameters count, straightforward effect
4) Full-order linearization, no zero dynamics
5) No need of cascaded loops

Note that points 4 and 5 together allow the use of an arbitrarily fast control dynamics, limited only by noise concerns, as it removes the ”frequency separation” constraints. As flat systems have a state-free inverse, the ideal trajectory tracking is instantaneous through a feedforward-only controller. To compensate disturbances, modeling errors and initial state errors, a feedback gain is introduced. On the other hand, as DFT-based control relies on exact feedforward, it requires a good knowledge of the system. A trajectory planning principle that keeps the physical meaning and with reasonable assumptions will be presented. An other drawback of this kind of control is its lack of system protection compared to cascaded controllers. The trajectories can be chosen such that the safe operating area is never exceeded in normal operation, but an excessive and unpredictable load (or a short-circuit) will inevitably push the system outside its limits, and taking corrective actions with a DFT-based control law is difficult[1]. This is not a problem for MMC, since capacitors are left floating and not directly exposed to the load.

To our knowledge, only a few applications of full-order non-linear control for MMC have been investigated. In [9], feedback linearization is used but no proof of global stabilization is given, and the resulting zero dynamics reduces overall performance. In [15], the formalism of flatness-based control was used, but the MMC was treated as a simple inverter - the stabilization of its own state variables was not presented nor achieved through differential flatness formalism. The original contributions of our paper can be summarized as follows:

1) A proof of differential flatness property of the MMC;
2) A flat output proposition for the MMC;
3) A complete trajectory planning strategy, allowing active and reactive power tracking and capacitor voltage balancing;
4) A full-order, flatness-based controller for the MMC, with both a feedforward and a feedback action, ensuring theoretical global exponential stability (GES) of the operating point;
5) The validation of the proposed control scheme through Matlab/Simulink simulations with losses under strong measurement noises corresponding to a realistic case of on-shore, point-to-point HVDC interconnection.

The paper is organized as follows: in section II, the equivalent schematic and dynamic average model of the MMC is derived. A flat output is proposed for one arm and extended to the whole converter in section III, proving the differential flatness property of the MMC. In section IV, the trajectory generation for this flat output is detailed, resulting from high-level references (AC grid active and reactive power references). The proposed controller is presented in section V, through its linearization layer, feedforward action and feedback action. Aggregating all the previous results, section VI evaluates the performance of the proposed control scheme in simulation. Finally, section VII is dedicated to the conclusions and perspectives of this paper.

II. System Modelling

For the proposed work, the grid configuration shown in Fig. 2 is considered. It corresponds to a high-power, redundant VSC-HVDC corridor in bipolar configuration, with intermediate substations in symmetrical monopole configuration. This last choice has been made because of the lower cost and footprint, at the expense of redundancy - hence, only substations with either reduced power or lower strategic importance are configured as monopoles. These monopoles are connected across the DC lines : even though a metallic return is present, allowing asymmetric connections, having substation C connected between a DC pole and the metallic return (ground) would load the latter, cause an unbalance in substations A and B and increase the insulation constraint on the transformer in substation C.

[1]The feedback action will naturally tend to maintain or worsen the overload, for instance by regulating the output voltage of the converter during an excessive loading condition.

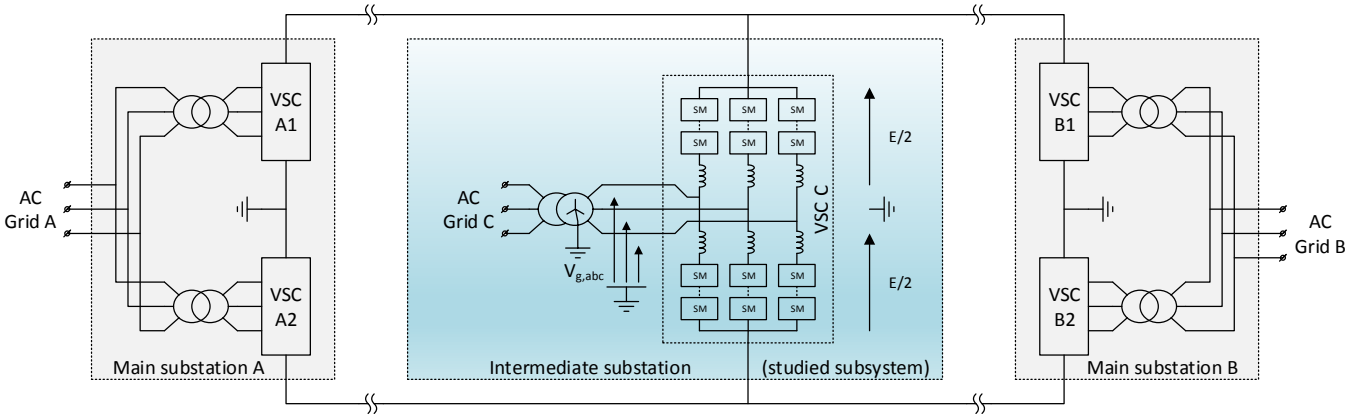

Fig. 2. Studied configuration. Only the substation C is modelled, others elements being assumed ideal.

In this paper, only VSC C is modelled and controlled and all outer elements are assumed ideal, corresponding to the assumption of strong AC and DC grids. E and $V_{g,abc}$ are, thus, modeled as ideal voltage sources.

As mentioned in Section I, a common method to reduce the MMC model order is the so-called "average" approach [5]. It relies on the assumption that every capacitor in a given stack have the same voltage, which is ensured by the low level controller. Defining a stack as the series assembly of submodules into each arm, each stack is replaced by a DC transformer whose ratio is the equivalent control input of the arm, feeding an equivalent capacitor. This ratio is called the modulation index of the arm, noted m. Applying this approach to the original converter, the resulting schematic is given in Fig. 3. All the parameters correspond to those in this figure, and the resulting model is similar to the one used in [16].

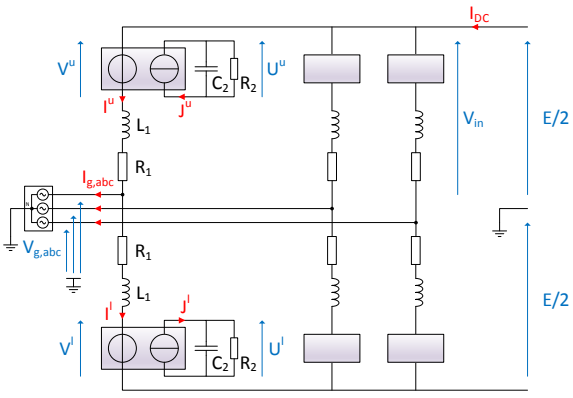

Fig. 3. MMC - Equivalent average schematic. Indices a, b and c are omitted for clarity purposes.

Using the notations of Fig. 3, m corresponds to the ratio of V to U (for instance, $m_a^u = V_a^u/U_a^u$). For modeling and control purposes, the state and control vectors are respectively given in (1) and (2). The former is composed of the six arm inductor currents and the six arm equivalent capacitor voltages, whereas the latter is made of the six modulation indexes of the arms. The superscripts "u" and "l" are used for the upper and lower arms and the subscripts "a, b, c" correspond to phase legs.

$$\begin{aligned} x &= \left[I_a^u, U_a^u, I_a^l, U_a^l, I_b^u, U_b^u, I_b^l, U_b^l, I_c^u, U_c^u, I_c^l, U_c^l\right]^T \\ &:= \left[x_1, x_2, x_3, x_4, x_5, x_6, x_7, x_8, x_9, x_{10}, x_{11}, x_{12}\right]^T \end{aligned} \tag{1}$$

$$\begin{aligned} u &= \left[m_a^u, m_a^l, m_b^u, m_b^l, m_c^u, m_c^l\right]^T \\ &:= \left[u_1, u_2, u_3, u_4, u_5, u_6\right]^T \end{aligned} \tag{2}$$

The model is presented under the so-called MIMO control-affine form, $\dot{x} = f(x) + G(x)u$, where $f(x)$ and $G(x)$ are detailed in (3) and (4) with $G(x)$ defined as $\begin{bmatrix} g_1(x) & \cdots & g_6(x) \end{bmatrix}$. As the considered output depends on the control strategy, no output equation is given at this step.

$$f(x) = \begin{bmatrix} \frac{E}{2L_1} - \frac{V_{ga}}{L_1} - \frac{R_1 \cdot x_1}{L_1} \\ \frac{-x_2}{R_2 \cdot C_2} \\ \frac{E}{2L_1} + \frac{V_{ga}}{L_1} - \frac{R_1 \cdot x_3}{L_1} \\ \frac{-x_4}{R_2 \cdot C_2} \\ \frac{E}{2L_1} - \frac{V_{gb}}{L_1} - \frac{R_1 \cdot x_5}{L_1} \\ \frac{-x_6}{R_2 \cdot C_2} \\ \frac{E}{2L_1} + \frac{V_{gb}}{L_1} - \frac{R_1 \cdot x_7}{L_1} \\ \frac{-x_8}{R_2 \cdot C_2} \\ \frac{E}{2L_1} - \frac{V_{gc}}{L_1} - \frac{R_1 \cdot x_9}{L_1} \\ \frac{-x_{10}}{R_2 \cdot C_2} \\ \frac{E}{2L_1} + \frac{V_{gc}}{L_1} - \frac{R_1 \cdot x_{11}}{L_1} \\ \frac{-x_{12}}{R_2 \cdot C_2} \end{bmatrix} \tag{3}$$

$$G(x) = \begin{bmatrix} \frac{-x_2}{L_1} & 0 & 0 & 0 & 0 & 0 \\ \frac{x_1}{C_2} & 0 & 0 & 0 & 0 & 0 \\ 0 & \frac{-x_4}{L_1} & 0 & 0 & 0 & 0 \\ 0 & \frac{x_3}{C_2} & 0 & 0 & 0 & 0 \\ 0 & 0 & \frac{-x_6}{L_1} & 0 & 0 & 0 \\ 0 & 0 & \frac{x_5}{C_2} & 0 & 0 & 0 \\ 0 & 0 & 0 & \frac{-x_8}{L_1} & 0 & 0 \\ 0 & 0 & 0 & \frac{x_7}{C_2} & 0 & 0 \\ 0 & 0 & 0 & 0 & \frac{-x_{10}}{L_1} & 0 \\ 0 & 0 & 0 & 0 & \frac{x_9}{C_2} & 0 \\ 0 & 0 & 0 & 0 & 0 & \frac{-x_{12}}{L_1} \\ 0 & 0 & 0 & 0 & 0 & \frac{x_{11}}{C_2} \end{bmatrix} \tag{4}$$

The previous quantities are defined over the following space[2], where $i \in \mathbb{N}$, $i = 1, \ldots, 6$:

$$x_{2i-1} \in \mathbb{R} \ , \ x_{2i} \in \mathbb{R}^+ \backslash \{0\} \ , \ u_i \in [0, +1] \tag{5a}$$

$$R_1, R_2, L_1, C_2 \in \mathbb{R}^+ \ , \ V_{g,abc} \in \left(-\frac{E}{2}, +\frac{E}{2}\right) \tag{5b}$$

III. Flat output determination

As it was demonstrated in [17], the MMC averaged model of Fig. 3 configuration exhibits an arm-decoupled behaviour. The flat output determination will thus be performed on one arm, and verified on the complete system.

A. Flat output construction for a single arm

By definition, a flat system can be changed into a linear system through the use of an endogenous feedback and a change of coordinates [18], the new state vector being composed of the flat output and its time-derivatives. As a consequence, both state and control vectors can be expressed using the latter. It is strongly related to full-order feedback linearization, which is described in [19]. More information about this equivalence are given in [20].

In the particular case where the relative degree of the system is equal to the system's order, the input–output linearization becomes equivalent to the input-state linearization of the system [25, p.34]. Thus, a necessary and sufficient condition of flatness for a SISO (single-input, single-output) system of state equation $\dot{x} = f(x) + g(x)u$ and a candidate output $\lambda(x)$ is given in (6), where n is the system order, $L_f g(x) = [\vec{\nabla} g(x)] \cdot f(x)$ is the Lie derivative of $g(x)$ along $f(x)$, and $L_g^k f(x) = L_g[L_g^{k-1} f(x)]$ is the iterated Lie derivative [19].

$$L_g L_f^{k-1} \lambda(x) = 0 \ , \quad k < n \tag{6a}$$

$$L_g L_f^{k-1} \lambda(x) \neq 0 \ , \quad k = n \tag{6b}$$

As each arm is connected between two voltage sources, both may be combined to obtain a general reduced equation. This differential voltage, V_{in}, is defined as the difference between top and bottom voltages of each arm. As an illustration, for the upper arm of phase a, V_{in} equals $E/2 - V_{ga}$. Defined $\bar{x}$ as the sub-vector of x contained the inductor current and the equivalent capacitor voltage of an arm and $\bar{u}$ the corresponding modulation index, it can be seen, from (3), that V_{in} appears clearly in this model. The arm dynamics can then be generalized, independently of its position inside the converter, as a second-order, SISO, affine subsystem (7).

$$\dot{\bar{x}} = \bar{f}(\bar{x}) + \bar{g}(\bar{x})\bar{u} = \begin{bmatrix} \frac{V_{in}}{L_1} - \frac{R_1 \cdot \bar{x}_1}{L_1} \\ -\frac{\bar{x}_2}{R_2 \cdot C_2} \end{bmatrix} + \begin{bmatrix} -\frac{\bar{x}_2}{L_1} \\ \frac{\bar{x}_1}{C_2} \end{bmatrix} \cdot \bar{u} \tag{7}$$

For a given MMC arm, taking into account the time-varying nature of V_{in}, the condition (6a) implies that:

$$\frac{\bar{x}_2}{L_1} \frac{\partial \lambda(\bar{x})}{\partial \bar{x}_1} = \frac{\bar{x}_1}{C_2} \frac{\partial \lambda(\bar{x})}{\partial \bar{x}_2} \tag{8}$$

[2]The capacitor voltages are physically limited to a much higher value than 0 because of the SM anti-parallel diodes, which act as a diode rectifier. This effect allows, by the way, the start-up (precharge) procedure of the MMC.

An obvious solution to this partial derivative equation is given in (9), where $K \in \mathbb{R} \backslash \{0\}$ is an arbitrary constant.

$$\lambda(\bar{x}) = \frac{K \bar{x}_1^2}{2C_2} + \frac{K \bar{x}_2^2}{2L_1} \tag{9}$$

Condition (6b) can now be checked. The computation gives:

$$L_{\bar{g}} L_{\bar{f}} \lambda(\bar{x}) = -\frac{K V_{in} \bar{x}_2}{L_1^2 C_2} + \frac{2K R_1 \bar{x}_1 \bar{x}_2}{L_1^2 C_2} - \frac{2K \bar{x}_1 \bar{x}_2}{R_2 L_1 C_2^2} \tag{10}$$

A singularity exists: $L_{\bar{g}} L_{\bar{f}} \lambda(\bar{x})$ is null for $\bar{x}_1 = \frac{V_{in}}{2L_1} \frac{\tau_1 \tau_2}{\tau_2 - \tau_1}$, where $\tau_1 = L_1/R_1$ and $\tau_2 = R_2 C_2$ are the time constants of both storage elements. However, for the case study presented after, these singularities appear far beyond the physical domain. So both conditions (6) are verified for the physical domain and consequently, the MMC arm is differentially flat and $\lambda(\bar{x})$ is a flat output for this subsystem. The relative degree ρ of the output $\lambda(\bar{x})$ is two. According the the aforementioned properties of flat systems, both u and x can be expressed as a function of λ and its time-derivatives, as presented in (11), neglecting R_1 and R_2 for conciseness.

$$\begin{aligned} x_1 &= \frac{L_1 C_2}{K V_{in}(t)} \dot{\lambda}(t) \\ x_2 &= \left(\frac{2L_1}{K} \lambda(t) - \frac{L_1^2}{K V_{in}^2(t)} \dot{\lambda}(t)^2 \right)^{1/2} \\ u &= \frac{V_{in}(t) + \frac{L_1^2 C_2 \dot{V}_{in}(t)}{K V_{in}^2(t)} \dot{\lambda}(t) - \frac{L_1^2 C_2}{K V_{in}(t)} \ddot{\lambda}(t)}{\left(\frac{2L_1}{K} \lambda(t) - \frac{L_1^2}{K V_{in}^2(t)} \dot{\lambda}(t)^2 \right)^{1/2}} \end{aligned} \tag{11}$$

B. Extension to the MIMO system

From the results of the previous section, a proposed flat output vector $\Lambda(x)$ for the global system is presented in (12).

$$\Lambda(x) = \begin{bmatrix} \lambda_1(x) \\ \vdots \\ \lambda_6(x) \end{bmatrix} = K \cdot \begin{bmatrix} \frac{x_1^2}{2C_2} + \frac{x_2^2}{2L_1} \\ \frac{x_3^2}{2C_2} + \frac{x_4^2}{2L_1} \\ \frac{x_5^2}{2C_2} + \frac{x_6^2}{2L_1} \\ \frac{x_7^2}{2C_2} + \frac{x_8^2}{2L_1} \\ \frac{x_9^2}{2C_2} + \frac{x_{10}^2}{2L_1} \\ \frac{x_{11}^2}{2C_2} + \frac{x_{12}^2}{2L_1} \end{bmatrix} \tag{12}$$

The analysis shows that $\forall (i,j) \in \mathbb{N}^2 \ , \ i,j = 1, ..., 6$, the properties (13) are verified. They constitute a sufficient condition of differential flatness for the MMC converter in the physical domain.

$$L_{g_i} \lambda_j(x) = 0 \tag{13a}$$

$$L_{g_i} L_f \lambda_j(x) = 0 \ , \quad i \neq j \tag{13b}$$

$$L_{g_i} L_f \lambda_j(x) \neq 0 \ , \quad i = j \tag{13c}$$

As for a single arm, the relative degree ρ_i of the output λ_i is two, so $\sum_{i=1}^{6} \rho_i = 12 = n$. The complet MMC is differentially flat with flat output λ_i, $i = 1, ..., 6$.

IV. Trajectory planning

The trajectory vector for $\Lambda(x)$, called $Y(t)$, is composed of six individual trajectories $y_i(t)$ as $\Lambda(x)$ itself. Since the relative degree of each output component is two, a trajectory such that $Y(t)$ and $\dot{Y}(t)$ are continuous functions is reachable at any time with a finite (but sometimes discontinuous) control action $u(t)$.

The proposed trajectory generation principle relies on the following observation: for a suitable choice of K, namely $K = L_1C_2$, each flat output component $\lambda_i(x)$ describes the total stored energy into the $i-th$ MMC arm, as shown in (14).

$$\lambda_i(x) = \frac{1}{2}L_1x_{2i-1}^2 + \frac{1}{2}C_2x_{2i}^2 \tag{14}$$

To ease the link with this physical interpretation, for an arm i, $y_i(t)$ will be noted $e_i(t)$ (energy) in this section, such as $p_i(t) = {y_i}^{(1)}(t)$ (power) and $\dot{p}_i(t) = {y_i}^{(2)}(t)$ (power derivative).

A. Instantaneous power

The three-phase AC grid voltage expression is presented in (15), where ω is the grid angular frequency and $\hat{V}_g$ is the line-to-neutral peak voltage of the AC grid.

$$\begin{bmatrix} V_{g,a} \\ V_{g,b} \\ V_{g,c} \end{bmatrix} = \begin{bmatrix} \hat{V}_g \cdot \cos(\omega t - \frac{0\pi}{3}) \\ \hat{V}_g \cdot \cos(\omega t - \frac{2\pi}{3}) \\ \hat{V}_g \cdot \cos(\omega t - \frac{4\pi}{3}) \end{bmatrix} \tag{15}$$

The resulting six arm voltages V_{in_i} are given in (16).

$$V_{in_i} = \frac{E}{2} - \hat{V}_g \cdot \cos(\omega t + \theta_i)\ ,\ \theta_i = \begin{cases} 0\pi/3\ , & i = 1 \\ 3\pi/3\ , & i = 2 \\ 4\pi/3\ , & i = 3 \\ 1\pi/3\ , & i = 4 \\ 2\pi/3\ , & i = 5 \\ 5\pi/3\ , & i = 6 \end{cases} \tag{16}$$

First of all, the active and reactive power references are translated into instantaneous current references. The AC grid current reference is purely sinusoidal and has two components, an active and a reactive one. The active and reactive powers, P_{ref} and Q_{ref} are defined for the whole converter and each arm has the same contribution. Moreover, a DC component is required in each arm, flowing vertically inside the converter, to ensure energy balance inside the converter. After neglecting the losses[3], the instantaneous current trajectory inside each arm is obtained and given in (17) [17].

$$I_i^r = \frac{P_{ref}(t)}{3E} + \frac{P_{ref}(t)\cos(\omega t + \theta_i)}{3\hat{V}_g} + \frac{Q_{ref}(t)\sin(\omega t + \theta_i)}{3\hat{V}_g} \tag{17}$$

The instantaneous power can now be computed, decomposed as (18):

$$p_i(t) = V_{in_i}(t) \cdot I_i^r(t) = P_{ref}(t) \cdot \gamma_{P_i}(t) + Q_{ref}(t) \cdot \gamma_{Q_i}(t) \tag{18}$$

[3]It corresponds to energy conservation hypothesis, with powers at each terminal being equal. As the efficiency of a full-scale MMC is typically around 99%, this hypothesis seems realistic.

With:

$$\gamma_{P_i}(t) = \frac{1}{6} + \left(\frac{E}{6\hat{V}_g} - \frac{\hat{V}_g}{3E} - \frac{\cos(\omega t + \theta_i)}{3}\right)\cos(\omega t + \theta_i) \tag{19a}$$

$$\gamma_{Q_i}(t) = \left(\frac{E}{6\hat{V}_g} - \frac{\cos(\omega t + \theta_i)}{3}\right)\sin(\omega t + \theta_i) \tag{19b}$$

B. Instantaneous power derivative

The expressions given in the previous sections are varying not only because of their harmonic terms (steady-state variation), but also because of the varying nature of $P_{ref}(t)$ and $Q_{ref}(t)$, which are given by the application. The inputs of the proposed controller contain not only $P_{ref}(t)$ and $Q_{ref}(t)$, but also $\dot{P}_{ref}(t)$ and $\dot{Q}_{ref}(t)$.

With this consideration and from the time-derivative of equation (18), $\dot{p}(t)$ is expressed in (20):

$$\begin{aligned} \dot{p}_i(t) = P_{ref}(t) \cdot \dot{\gamma}_{P_i}(t) + \dot{P}_{ref}(t) \cdot \gamma_{P_i}(t) + \\ Q_{ref}(t) \cdot \dot{\gamma}_{Q_i}(t) + \dot{Q}_{ref}(t) \cdot \gamma_{Q_i}(t) \end{aligned} \tag{20}$$

With:

$$\dot{\gamma}_{P_i}(t) = \left(-\frac{E\omega}{6\hat{V}_g} + \frac{\hat{V}_g\omega}{3E} + \frac{2\omega}{3}\cos(\omega t + \theta_i)\right)\sin(\omega t + \theta_i) \tag{21a}$$

$$\dot{\gamma}_{Q_i}(t) = \frac{E\omega\cos(\omega t + \theta_i)}{6\hat{V}_g} - \frac{\omega\cos(2\omega t + 2\theta_i)}{3} \tag{21b}$$

In order to have a finite $\dot{p}_i(t)$, $P_{ref}(t)$ and $Q_{ref}(t)$ have to be at least continuous.

C. Instantaneous energy

$e_i(t)$ is the time-integral of $p_i(t)$, but the non-deterministic nature of $P_{ref}(t)$ and $Q_{ref}(t)$ eliminates the possibility of an analytical calculation. This integration will be calculated as (22), where E_0 corresponds to the average value of $e_i(t)$ over a $2\pi/\omega$ period.

$$e_i(t) = \int_0^t p_i(\tau)d\tau + E_0 \tag{22}$$

Indirectly, as the energy is clearly dominated by its capacitive component, with an average value almost equal to $1/2C_2U_i^2$, E_0 is directly linked with the average arm capacitor voltage U_i, which is of prime interest.

V. Flatness-based control

As the total losses are around 1% of the nominal power for a real MMC [21] (see footnote 3), as explained before, they may be negligeable and all the controller design will be made under the assumption of zero-losses (thus $R_1 = 0$ and $1/R_2 = 0$). It greatly simplifies the calculation by giving an unique solution[4]. This assumption should be relevant for the

[4]If the losses are taken into account, several second-degree equations are involved in the calculations, and the determination of the meaningful solution is not always straightforward

control design. Its validity will be tested in the simulation results, where a lossy model is used.

The flatness-based controller contains both a feedback and a feed-forward action, applied through a trajectory-based linearization layer.

A. Linearization layer

The role of this layer, which is based on feedback linearization theory, is to reconstruct the physical control u from the state vector x and a pseudo-control v using a change of coordinates $z = \Phi(x)$ and a feedback control $u(x, v)$, such that the transformed system is linear and decoupled. For a general MIMO flat system with n states and m inputs, $\dot{z} = \sigma + \tau v$ is composed only of integrator chains where σ and τ are given by:

$$\sigma = \begin{bmatrix} \begin{bmatrix} 0 & 1 \\ & \ddots & \\ 0 & & 0 \end{bmatrix} & & 0 \\ & \ddots & \\ 0 & & \begin{bmatrix} 0 & 1 \\ & \ddots & \\ 0 & & 0 \end{bmatrix} \end{bmatrix}, \quad \tau = \begin{bmatrix} \begin{bmatrix} 0 \\ \vdots \\ 1 \end{bmatrix} & & 0 \\ & \ddots & \\ 0 & & \begin{bmatrix} 0 \\ \vdots \\ 1 \end{bmatrix} \end{bmatrix} \tag{23}$$

The control law $u(x, v)$ is written under the form (24). Its components are detailed in (25) and (26) [19].

$$u(x, v) = \Delta(x)^{-1} \cdot (-\Gamma(x) + v) \tag{24}$$

$$\Delta(x) = \begin{bmatrix} L_{g_1} L_f^{\rho_1 - 1} \lambda_1(x) & \cdots & L_{g_1} L_f^{\rho_m - 1} \lambda_m(x) \\ \vdots & \ddots & \vdots \\ L_{g_n} L_f^{\rho_1 - 1} \lambda_1(x) & \cdots & L_{g_n} L_f^{\rho_m - 1} \lambda_m(x) \end{bmatrix} \tag{25}$$

$$\Gamma(x) = \begin{bmatrix} L_f^{\rho_1} \lambda_1(x) & \cdots & L_f^{\rho_m} \lambda_m(x) \end{bmatrix}^T \tag{26}$$

For the MMC, $\Delta(x)$ and $\Gamma(x)$ are shown in (27).

$$\Delta(x) = -\frac{1}{L_1} \begin{bmatrix} V_{in_1} x_2 & 0 & 0 & 0 & 0 & 0 \\ 0 & V_{in_2} x_4 & 0 & 0 & 0 & 0 \\ 0 & 0 & V_{in_3} x_6 & 0 & 0 & 0 \\ 0 & 0 & 0 & V_{in4} x_8 & 0 & 0 \\ 0 & 0 & 0 & 0 & V_{in_5} x_{10} & 0 \\ 0 & 0 & 0 & 0 & 0 & V_{in_6} x_{12} \end{bmatrix} \tag{27a}$$

$$\Gamma(x) = \begin{bmatrix} V_{in_1}^2 / L_1 + \dot{V}_{in_1} x_1 \\ V_{in_2}^2 / L_1 + \dot{V}_{in_2} x_3 \\ V_{in_3}^2 / L_1 + \dot{V}_{in_3} x_5 \\ V_{in_4}^2 / L_1 + \dot{V}_{in_4} x_7 \\ V_{in_5}^2 / L_1 + \dot{V}_{in_5} x_9 \\ V_{in_6}^2 / L_1 + \dot{V}_{in_6} x_{11} \end{bmatrix} \tag{27b}$$

The change of coordinates is defined in (28) for a general MIMO system and in (29) for the MMC.

$$\Phi(x) = \begin{bmatrix} \lambda_1(x) \\ L_f \lambda_1(x) \\ \vdots \\ L_f^{\rho_1 - 1} \lambda_1(x) \\ \vdots \\ \vdots \\ \lambda_n(x) \\ L_f \lambda_n(x) \\ \vdots \\ L_f^{\rho_n - 1} \lambda_n(x) \end{bmatrix} \tag{28}$$

$$\Phi(x) = \begin{bmatrix} \lambda_1(x) \\ \dot{\lambda}_1(x) \\ \lambda_2(x) \\ \dot{\lambda}_2(x) \\ \lambda_3(x) \\ \dot{\lambda}_3(x) \\ \lambda_4(x) \\ \dot{\lambda}_4(x) \\ \lambda_5(x) \\ \dot{\lambda}_5(x) \\ \lambda_6(x) \\ \dot{\lambda}_6(x) \end{bmatrix} = \begin{bmatrix} 1/2 \cdot \left(L_1 x_1^2 + C_2 x_2^2 \right) \\ V_{in_1} \cdot x_1 \\ 1/2 \cdot \left(L_1 x_3^2 + C_2 x_4^2 \right) \\ V_{in_2} \cdot x_3 \\ 1/2 \cdot \left(L_1 x_5^2 + C_2 x_6^2 \right) \\ V_{in_3} \cdot x_5 \\ 1/2 \cdot \left(L_1 x_7^2 + C_2 x_8^2 \right) \\ V_{in_4} \cdot x_7 \\ 1/2 \cdot \left(L_1 x_9^2 + C_2 x_{10}^2 \right) \\ V_{in_5} \cdot x_9 \\ 1/2 \cdot \left(L_1 x_{11}^2 + C_2 x_{12}^2 \right) \\ V_{in_6} \cdot x_{11} \end{bmatrix} \tag{29}$$

The Jacobian matrix $\mathcal{J}_{\Phi(x)} = \left[\frac{\partial \Phi(x)}{\partial x} \right]$ of this change of coordinates is not shown for reasons of conciseness, but its determinant is given in (30):

$$\det \mathcal{J}_{\Phi(x)} = C_2^6 \cdot \prod_{k=1}^{6} \left(V_{in_k} x_{2k} \right) \tag{30}$$

Using the domain defined in (5), it can be seen that neither x_{2k} or V_{in_k} reach zero, so the determinant of (30) never reaches zero either. Consequently the change of coordinates $\Phi(x)$ is a diffeomorphism, which was intuited through the flatness property of $\Lambda(x)$. Its inverse is then defined, and given in (31).

$$\Phi^{-1}(z) = \begin{bmatrix} z_2 / V_{in_1} \\ 1/\sqrt{C_2} \cdot \left(2 z_1 - L_1 z_2^2 / V_{in_1}^2 \right)^{1/2} \\ z_4 / V_{in_2} \\ 1/\sqrt{C_2} \cdot \left(2 z_3 - L_1 z_4^2 / V_{in_2}^2 \right)^{1/2} \\ z_6 / V_{in_3} \\ 1/\sqrt{C_2} \cdot \left(2 z_5 - L_1 z_6^2 / V_{in_3}^2 \right)^{1/2} \\ z_8 / V_{in_4} \\ 1/\sqrt{C_2} \cdot \left(2 z_7 - L_1 z_8^2 / V_{in_4}^2 \right)^{1/2} \\ z_{10} / V_{in_5} \\ 1/\sqrt{C_2} \cdot \left(2 z_9 - L_1 z_{10}^2 / V_{in_5}^2 \right)^{1/2} \\ z_{12} / V_{in_6} \\ 1/\sqrt{C_2} \cdot \left(2 z_{11} - L_1 z_{12}^2 / V_{in_6}^2 \right)^{1/2} \end{bmatrix} \tag{31}$$

It can be noted that the quantities found under the square root are always positive since the MMC requires a sufficiently high

reference voltage on the capacitors. From these expressions, the linearizing control law can be calculated. The combination of (24) and (31) gives the flatness-based control law, where the linearization layer makes use of trajectories instead of measurements. To do so, x is replaced by its trajectory x_{traj} determined by (32).

$$x_{traj} = \Phi^{-1}(z_{traj}) \tag{32a}$$

$$z_{traj} = [y_1 \ \dot{y}_1 \ \cdots \ y_6 \ \dot{y}_6]^T \tag{32b}$$

B. Feedforward and feedback action

The pseudo-control v contains a feedforward action and a feedback action. The feedforward action is taken from the ρ-th derivative of the trajectory, as shown in (33) for a general MIMO system.

$$v_{FF} = \begin{bmatrix} y_1^{(\rho_1)} & y_2^{(\rho_2)} & \cdots & y_m^{(\rho_m)} \end{bmatrix}^T \tag{33}$$

The expression for MMC is shown in (34) since $\rho_i = 2$ for $i = 1, ..., 6$.

$$v_{FF} = \begin{bmatrix} \ddot{y}_1 & \ddot{y}_2 & \ddot{y}_3 & \ddot{y}_4 & \ddot{y}_5 & \ddot{y}_6 \end{bmatrix}^T \tag{34}$$

The feedback action is the only term which makes use of the output measurements z. Assuming that the operating point lies on the trajectory (i.e. $\Lambda(x) = Y$), a corrective action (35) is proposed, where $K_{FB} \in \mathbb{R}^{m \times n}$. It acts as a nonlinear proportional-derivative[5] controller on $\delta z = z_{traj} - z$.

$$v_{FB}(x) = K_{FB} \cdot \delta z = K_{FB} \cdot (z_{traj} - \Phi(x)) \tag{35}$$

It can be demonstrated that around the trajectory, the system dynamics is described by $\dot{\delta z} = (A - BK_{FB}) \cdot \delta z$, with:

$$A = \begin{bmatrix} \begin{bmatrix} 0 & 1 \\ 0 & 0 \end{bmatrix} & & 0 \\ & \ddots & \\ 0 & & \begin{bmatrix} 0 & 1 \\ 0 & 0 \end{bmatrix} \end{bmatrix}, \quad B = \begin{bmatrix} \begin{bmatrix} 0 \\ 1 \end{bmatrix} & & 0 \\ & \ddots & \\ 0 & & \begin{bmatrix} 0 \\ 1 \end{bmatrix} \end{bmatrix} \tag{36}$$

It corresponds to six independent chain of two integrators, as expected, and the pair $[A, B]$ is inherently controllable, implying that the 12 closed-loop poles (eigenvalues of $A - BK_{FB}$) can be chosen arbitrarily. Even though the number of solutions is infinite[6], to maintain the decoupled behavior given by the flatness-based control law, and to obtain the same dynamics in each arm, the following gain matrix is used:

$$K_{FB} = \begin{bmatrix} K_e & K_p & 0 & 0 & 0 & 0 & 0 & 0 & 0 & 0 & 0 & 0 \\ 0 & 0 & K_e & K_p & 0 & 0 & 0 & 0 & 0 & 0 & 0 & 0 \\ 0 & 0 & 0 & 0 & K_e & K_p & 0 & 0 & 0 & 0 & 0 & 0 \\ 0 & 0 & 0 & 0 & 0 & 0 & K_e & K_p & 0 & 0 & 0 & 0 \\ 0 & 0 & 0 & 0 & 0 & 0 & 0 & 0 & K_e & K_p & 0 & 0 \\ 0 & 0 & 0 & 0 & 0 & 0 & 0 & 0 & 0 & 0 & K_e & K_p \end{bmatrix} \tag{37}$$

[5]The derivative action comes from a proportional feedback on the 6 even state variables, which are the derivatives of the 6 odd ones, from the structure of $\Phi(x)$.

[6]K_{FB} is a $[6 \times 12]$ matrix, having thus 72 degrees of freedom for only 12 equations in the eigenvalue assignment problem

The resulting closed-loop eigenvalues are given in (38).

$$\begin{aligned} \text{eig}(A - BK_{FB}) &= \{\eta_1; \eta_2; \eta_1; \eta_2; \eta_1; \eta_2; \eta_1; \eta_2; \eta_1; \eta_2; \eta_1; \eta_2\} \\ \eta_1 &= -\frac{1}{2} \cdot \left(K_p + \sqrt{K_p^2 - 4K_e} \right) \\ \eta_2 &= -\frac{1}{2} \cdot \left(K_p - \sqrt{K_p^2 - 4K_e} \right) \end{aligned} \tag{38}$$

It is fundamental to notice that these eigenvalues do not describe the planned trajectory dynamics. Their role is only to reach the trajectory from a possibly unknown initial state, and to force the system to remain on it during operation despite the unmodelled disturbances. The ideal planned trajectory dynamics is governed only by the nature of $P_{ref}(t)$, $\dot{P}_{ref}(t)$, $Q_{ref}(t)$ and $\dot{Q}_{ref}(t)$. This kind of control law is able to follow instantly an arbitrary trajectory, as long as it is mathematically (required continuity class) and physically (actuator saturation) feasible. K_{FB} should be set as low as possible, whereas control gains are generally set as large as possible for classical control laws to improve tracking performance. An intuitive explanation for this property would be the following: the feedforward action governs the system perfectly as long as it is on the trajectory, and the feedback action ensures that it never strays from it.

C. Global control law

The two formed expressions are used to construct $v = v_{FF} + v_{FB}$, then v is applied through the linearization layer and u is obtained. Combining all the elements, the global flatness-based control scheme is shown in Fig. 4.

As the flat output is free from zero dynamics, the typical right-half-plane zero does not appear, neither does its inherent bandwidth limit. Moreover, the frequency separation constraint between loops that comes from classical cascaded control is also removed, since only one (second-order) controller is used per arm. The tuning of the gain is easy (only two parameters for the whole 12-th order system) and its consequence on the system behavior is straightforward. The theoretical global exponential stability of the operating point is guaranteed as the former eigenvalues lie into the open left half plane, thanks to DFT properties, because of the full-order linearization of the system.

VI. Simulation results

To validate the proposed control law, simulations based on a three-phase MMC average model have been made through Matlab/Simulink.

A. Simulation conditions

The simulation is done with Runge-Kutta 4 (ODE4) solver with 10μs of timestep. The parameters of the studied MMC, shown in Fig. 3, are summarized in Tab. I. It corresponds to a realistic case for on-shore, point-to-point HVDC interconnections. It can be noted that the losses are not neglected in the model in order to validate the robustness of the proposed control against parameter uncertainties. For a typical application, request active and reactive power references are constant

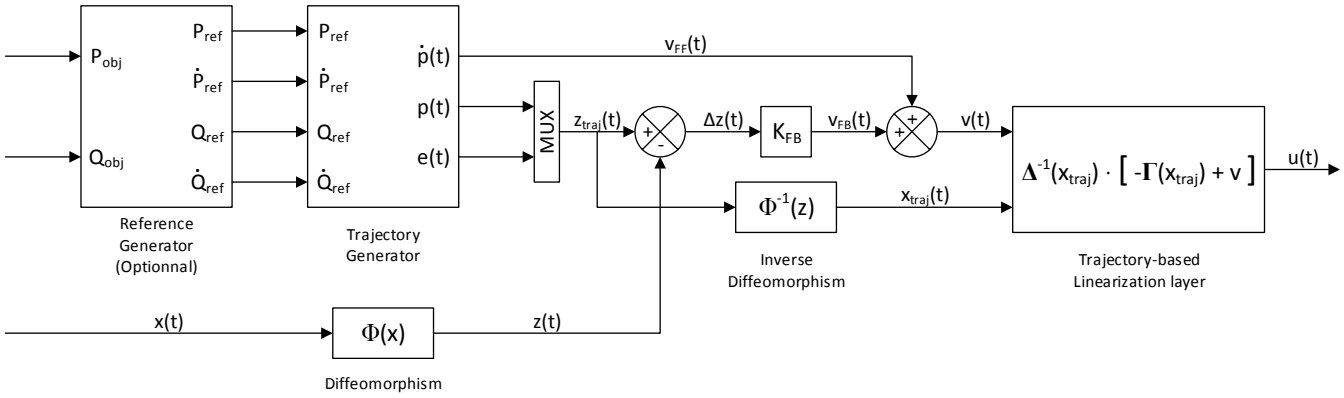

Fig. 4. Proposed control law schematic. The trajectory generator builds $\dot{p}(t) = [\dot{p}_1(t) \ \cdots \ \dot{p}_6(t)]^T$, $p(t) = [p_1(t) \ \cdots \ p_6(t)]^T$ and $e(t) = [e_1(t) \ \cdots \ e_6(t)]^T$ from (18), (20) and (22). The linearization layer is built on (27). The feedforward and feedback controllers are respectively based on (34) and (35).

TABLE I
SIMULATED MODEL PARAMETERS

Parameter	Value	Parameter	Value
E	640kV	L_1	50mH
$\hat{V}_g$	250kV	R_1	1Ω
S_n	1GVA	C_2	25μF
f_n	50Hz	R_2	1MΩ

in steady-state. To ensure $\mathcal{C}^1$ references, $\dot{P}_{ref}(t)$ and $\dot{Q}_{ref}(t)$ are defined first (piecewise-constant) and integrated. As shown in Fig. 5, active power reference changes between ± 800 MW and reactive power reference changes between ± 400 MVAR (nominal values). Each change is performed by a 20ms ramp.

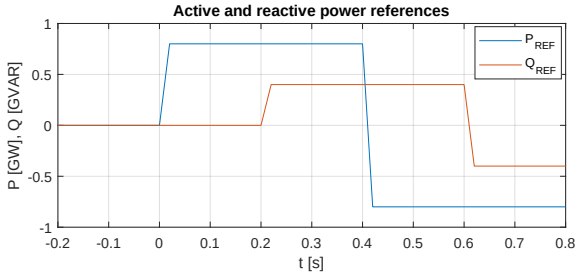

Fig. 5. Power references used into the simulations

B. Choice of the feedback gain

As mentioned previously, the feedback gain K_{FB} are determined by two control parameters K_e and K_p. They are chosen such that $\eta_1 = \eta_2 = -\omega_0$, leading to $K_p = 2\omega_0$ and $K_e = \omega_0^2$ according to (38).

To choose ω_0, a comparison is made under defined simulation conditions as in VI-A for $w_0 = 10\pi$, $w_0 = 100\pi$ and $w_0 = 1000\pi$, in both transient and steady-state conditions. Since in noise-free conditions, the feedback gain has only a minor impact on the overall performance, its choice will be made under strong measurement noise conditions.

To emulate the behaviour of both switching effects and actual measurement noises, a random noise is superimposed at the output of the converter model. It is built from a random number generator with a variance of 10^7 for the voltages and 10^2 for the currents. In both cases, the average value is 0 (no sensor offset) and the sampling time is equal to the simulation timestep ($10\mu s$). The seed of each generator is chosen equal to an arbitrary but different value in order to avoid unrealistic cancellations effects[7].

For a better visualization, only a zoom on a transient condition is shown, namely for $t \in [0.38, 0.40]$. For the level of noise involved, Fig. 6 shows the measurement of the arm currents and capacitor voltages.

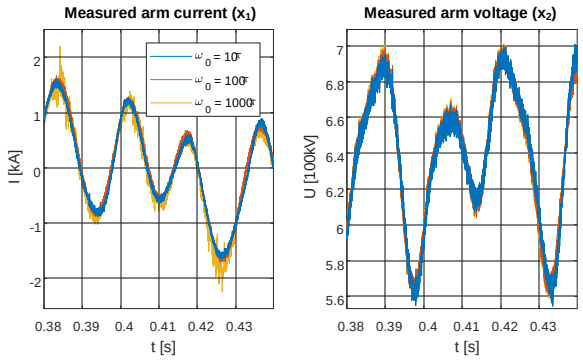

Fig. 6. Zoom of the current and voltage measurements with additional noise

Fig. 7 shows the control evolution of the upper arm of phase A. v_{FF} and v_{FB} are presented in the left-hand side of the figure, and u is shown on the right-hand side. The results enlighten the most important upper physical limit of the loop gain, as a high gain inexorably increases noise sensitivity. However, thanks to the intrinsic dynamic feedforward and linearization of flatness-based control, it is possible to use a low-enough gain from noise aspects, while allowing a good overall transient response and steady-state accuracy. With a feedback-only controller[8] and for given noise conditions, this tradeoff would impose a much stronger limit on the overall performance. For our example, $\omega_0 = 100\pi$ seen to be a good tradeoff choice and will be used for the following simulations.

[7]Typically, if the same noise is applied to I^u and I^l, then $I_{AC} = I^u - I^l$ and the active power P are noise-free

[8]Or feedback and static feedforward

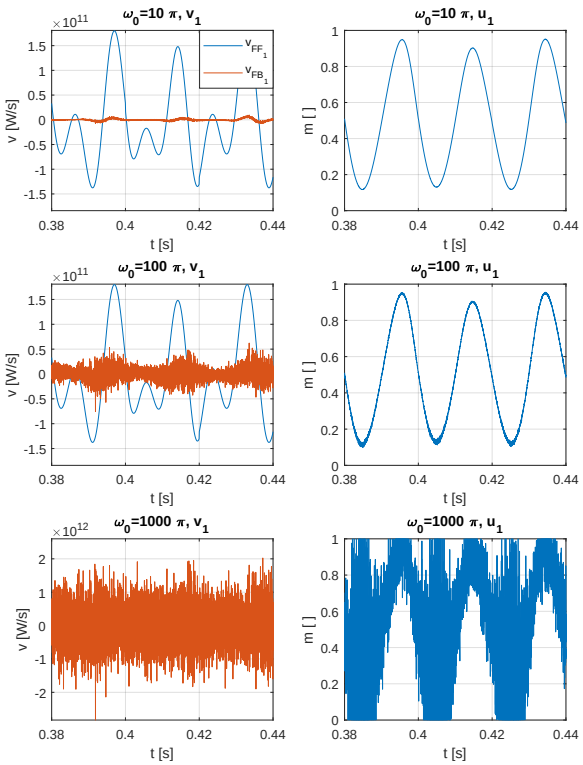

Fig. 7. Zoom of the control evolutions for 3 values of ω_0 with measurement noise

C. Power trajectory tracking performance

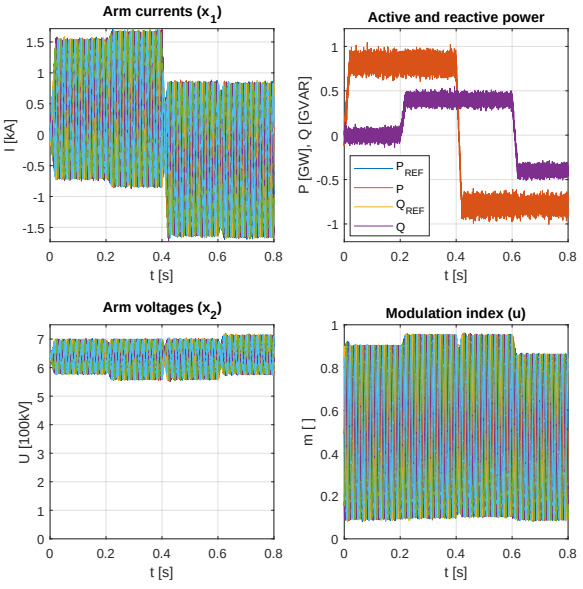

Fig. 8. Simulation results: nominal case, $P_{ref} = \pm 800$MW, $Q_{ref} = \pm 400$MVAR, 200ms stairs including 20ms ramps.

The tracking performance of the whole control is shown in Fig. 8, as the nominal power is established in only one grid period (20 ms). Small errors are present, mainly because R_1 and R_2 effects were neglected for the controller design. The average value of capacitor voltages is well controlled during these transients, with no perceptible undershot or overshoot.

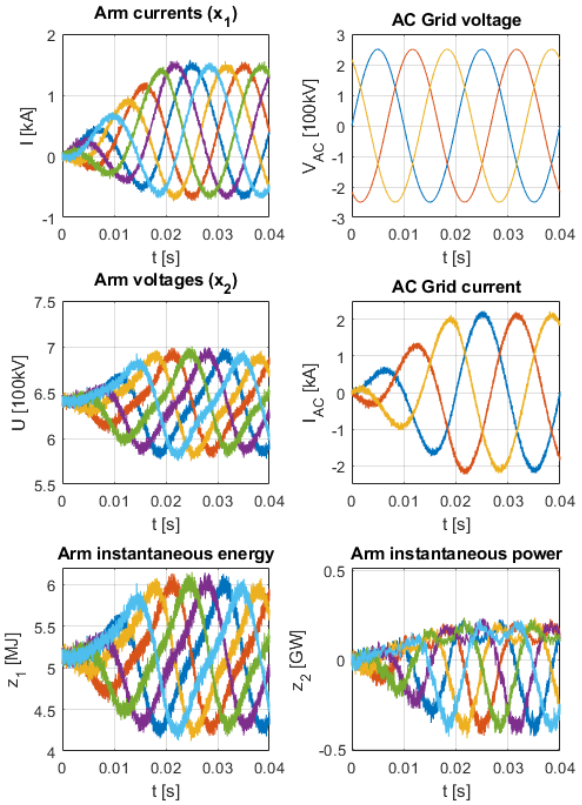

Fig. 9. Zoom for $t \in [0, 40ms]$

This constitutes a strength of the proposed control scheme, as fast response is ensured for all the state vector, and not only for an given internal (often current) loop. During this simulation, the modulation index m is always comprised between 0 and 1, hence no saturation effects are noticeable.

In Fig. 9, the shape of the 6 arm currents and capacitor voltages can be observed, with their DC component, whereas the steady-state condition ($t > 20ms$) allows to verify both the absence of DC component in $I_{g,abc}$ and its alignment with the corresponding grid voltage, $V_{g,abc}$, needed to operate at $P_{ref} \neq 0$, $Q_{ref} = 0$.

In order to better appreciate the obtained dynamic performance, the same simulation as Fig. 9 is performed without noise (Fig. 10).

VII. Conclusions and Perspectives

In this paper, the high-level control of a MMC is investigated. Based on the averaged model of MMC in its natural coordinates instead of the dq or Σ/Δ coordinates, the flatness property of an MMC arm has been proven, then extended to the full-order system. A trajectory planning method was proposed, and used to develop a full order, linearizing control law, thanks to differential flatness theory. Contrary to the state of the art, this method does not involve cascaded loop and it does not suffer from its common drawbacks, especially its need for frequency separation between the loops. Moreover, the theoretical global exponential stability is guaranteed thanks to DFT properties. Moreover, the proposed control system is simple to set since the number of tuning parameters is

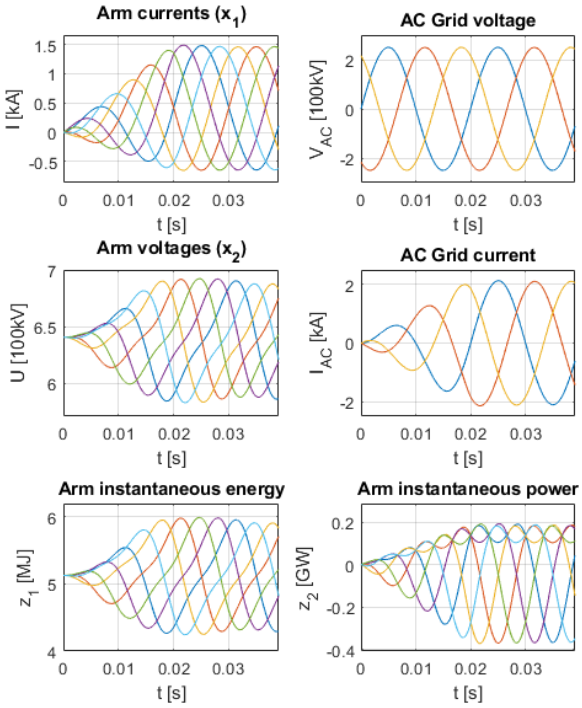

Fig. 10. Zoom for $t \in [0, 40ms]$, noise-free conditions

very low (2 in the proposed form). The proposed control was validated in simulation with measurement noise and modeling errors (presence of losses). The results show that the proposed control offers good performance with fast response for all the states, implying excellent dynamic response for both active and reactive powers.

Whereas the low sensitivity to losses (R_1 and R_2) of the proposed control was proven, no results were shown in the paper about the arm inductor (L_1) and the capacitor of the submodules (C_2) for the sake of conciseness. This study was conducted and shown that contrary to L_1, the sensitivity to C_2 could be an issue. Indeed the value of the capacitance can evolve during the converter operation due to aging and post-failure submodule elimination. Fortunately, C_2 is observable most of the time and its estimation is possible as shown in [22] [23]. Future works includes the combined use of the proposed control scheme and capacitance observer for both performance assessment and stability analysis. Moreover, detection of model inconsistencies and parametric changes with the use of a disturbance observer can be used. Finally, in the model of the converter, the impedance of the AC side (mainly due to the transformer) has been neglected. Taking into account this impedance is another work perspective.

REFERENCES

[1] R. H. Renner and D. Van Hertem, "Potential of using dc voltage restoration reserve for HVDC grids," *Electric Power Systems Research*, vol. 134, no. C, pp. 167–175, 2016.

[2] A. Lesnicar and R. Marquardt, "An innovative modular multilevel converter topology suitable for a wide power range," in *2003 IEEE Bologna Power Tech Conference Proceedings*, vol. 3, June 2003, pp. 6.

[3] V. Hofmann and M. Bakran, "A capacitor voltage balancing algorithm for hybrid modular multilevel converters in hvdc applications," in *2017 IEEE 12th International Conference on Power Electronics and Drive Systems (PEDS)*, Dec 2017, pp. 691–696.

[4] A. Zama, S. A. Mansour, D. Frey, A. Benchaib, S. Bacha, and B. Luscan, "A comparative assessment of different balancing control algorithms for modular multilevel converter (MMC)," in *2016 18th European Conference on Power Electronics and Applications (EPE'16 ECCE Europe)*, Sep. 2016, pp. 1–10.

[5] A. Antonopoulos, L. Angquist, and H. Nee, "On dynamics and voltage control of the modular multilevel converter," in *2009 13th European Conference on Power Electronics and Applications*, Sep. 2009, pp. 1–10.

[6] E. N. Abildgaard and M. Molinas, "Modelling and control of the modular multilevel converter (MMC)," *Energy Procedia*, vol. 20, pp. 227 – 236, 2012, technoport 2012 - Sharing Possibilities and 2nd Renewable Energy Research Conference (RERC2012).

[7] S. Samimi, F. Gruson, P. Delarue, and X. Guillaud, "Synthesis of different types of energy based controllers for a modular multilevel converter integrated in an hvdc link," in *11th IET International Conference on AC and DC Power Transmission*, Feb 2015, pp. 1–7.

[8] F. Abry, X. Brun, S. Sesmat, . Bideaux, and C. Ducat, "Electropneumatic cylinder backstepping position controller design with real-time closed-loop stiffness and damping tuning," *IEEE Transactions on Control Systems Technology*, vol. 24, no. 2, pp. 541–552, March 2016.

[9] Z. Li, Q. Hao, F. Gao, L. Wu, and M. Guan, "Nonlinear decoupling control of two-terminal mmc-hvdc based on feedback linearization," *IEEE Transactions on Power Delivery*, vol. 34, no. 1, pp. 376–386, Feb 2019.

[10] X. Brun and D. Thomasset, "Choice of control law in electropneumatics. expertise using an industrial benchmark and some new trends," in *Proceedings of the 39th IEEE Conference on Decision and Control (Cat. No.00CH37187)*, vol. 2, Dec 2000, pp. 1323–1328.

[11] A. Houari, H. Renaudineau, J. Martin, S. Pierfederici, and F. Meibody-Tabar, "Flatness-based control of three-phase inverter with output*lc*filter," *IEEE Transactions on Industrial Electronics*, vol. 59, no. 7, pp. 2890–2897, July 2012.

[12] A. Gensior, T. M. P. Nguyen, J. Rudolph, and H. Guldner, "Flatness-based loss optimization and control of a doubly fed induction generator system," *IEEE Transactions on Control Systems Technology*, vol. 19, no. 6, pp. 1457–1466, Nov 2011.

[13] C. Schmuck, F. Woittennek, A. Gensior, and J. Rudolph, "Feed-forward control of an hvdc power transmission network," *IEEE Transactions on Control Systems Technology*, vol. 22, no. 2, pp. 597–606, March 2014.

[14] M. Soheil-Hamedani, M. Zandi, R. Gavagsaz-Ghoachani, B. Nahid-Mobarakeh, and S. Pierfederici, "Flatness-based control method: A review of its applications to power systems," in *2016 7th Power Electronics and Drive Systems Technologies Conference (PEDSTC)*, Feb 2016, pp. 547–552.

[15] M. Mehrasa, E. Pouresmaeil, S. Taheri, I. Vechiu, and J. P. S. Catalão, "Novel control strategy for modular multilevel converters based on differential flatness theory," *IEEE Journal of Emerging and Selected Topics in Power Electronics*, vol. 6, no. 2, pp. 888–897, June 2018.

[16] G. Bergna-Diaz, D. Zonetti, S. Sanchez, R. Ortega, and E. Tedeschi, "PI passivity-based control and performance analysis of MMC multiterminal HVDC systems," *IEEE Journal of Emerging and Selected Topics in Power Electronics*, vol. 7, no. 4, pp. 2453–2466, Dec 2019.

[17] P.-B. Steckler, J.-Y. Gauthier, X. Lin-Shi, and F. Wallart, "Structural analysis and modular control law for modular multilevel converter (mmc)," in *ELECTRIMACS*, May 2019.

[18] M. Fliess, J. Levine, P. Martin, and P. Rouchon, "Flatness and defect of nonlinear systems: Introductory theory and examples," *International Journal of Control*, vol. 61, pp. 13–27, 06 1995.

[19] A. Isidori, *Nonlinear control systems*. Berlin New York: Springer, 1995.

[20] P. Martin, "On differentially flat systems," Theses, École Nationale Supérieure des Mines de Paris, Dec. 1992.

[21] B. Jacobson, P. Karlsson, G. Asplund, L. Harnefors, and T. Jonsson, "VSC-HVDC transmission with cascaded two-level converters," ABB Sweden, Tech. Rep., 2010.

[22] D. Ronanki and S. S. Williamson, "Health monitoring scheme for submodule capacitors in modular multilevel converter utilizing capacitor voltage fluctuations," in *IECON 2018 - 44th Annual Conference of the IEEE Industrial Electronics Society*, Oct 2018, pp. 2068–2073.

[23] F. Deng, Q. Wang, D. Liu, Y. Wang, M. Cheng, and Z. Chen, "Reference submodule based capacitor monitoring strategy for modular multilevel converters," *IEEE Transactions on Power Electronics*, vol. 34, no. 5, pp. 4711–4721, May 2019.

[24] M. Soheil-Hamedani, M. Zandi, R. Gavagsaz-Ghoachani, B. Nahid-Mobarakeh, and S. Pierfederici, "Flatness-Based Control Method: A Review of its applications to Power Systems," in *Electronics, Drive Systems & Technologies Conference (PEDSTC 2016)*, 16-18 Feb. 2016.
[25] G. Rigatos, *Nonlinear Control and Filtering Using Differential Flatness Approaches: Applications to Electromechanical Systems*, Springer International Publishing, 2015.